Applied Water Science (2022) 12:21
https://doi.org/10.1007/s13201-021-01555-6

ORIGINAL ARTICLE

End-of-life waste criteria: synthesis and utilization of Mn–Zn ferrite nanoparticles as a superparamagnetic photocatalyst for synergistic wastewater remediation

Maha A. Tony[1,2] · **M. M. Eltabey**[2]

Received: 6 August 2021 / Accepted: 10 December 2021 / Published online: 28 January 2022

Abstract

Dyes are toxic compounds that are widely included in industrial discharge. Their efficient and economical remediation can be explored through Fenton's oxidation. $Mn_{0.6}Zn_{0.4}Fe_2O_4$ nanoparticles are prepared via a simple and efficient co-precipitation technique and its chemical composition is confirmed through X-ray diffraction and its morphology via high-resolution transmission electron microscope. The prepared superparamagnetic photocatalyst based on $Mn_{0.6}Zn_{0.4}Fe_2O_4$ is applied for almost complete Synozol Blue dye removal (98% dye removal and 87% COD removal) and the results confirmed that the process is an efficient sustainable technique for the easily magnetically recoverable catalyst. Central composite design analysis was chosen to optimize the parametric conditions of the magnetized Fenton's variables through 13-level of a quadratic model. The optimized system variables were attained at 39 and 404 mg L^{-1} for catalyst and H_2O_2, respectively, at pH 3.0 with model correlation coefficients over than 98%. Recover and reuse are a viable option for 'close the loop' waste after final treatment as an 'end-of-life' waste potential and high removal efficiency is attained up to the 8^{th} cycle of catalyst reuse. Kinetics of Synozol Blue oxidation fitted through the first-order kinetic model. Finally, the thermodynamic parameters values concluded that the process is non-spontaneous and endothermic in nature.

Keywords Magnetic nanomaterials · Synozol blue wastewater · Photocatalysis · Central composite design · Kinetics · Thermodynamic parameters

Introduction

Water is a finite resource that becomes in deficiency due to the increasingly modern activities exist in our societies (Ercin and Hoekstra 2014; Ashour et al. 2014). Estimates by Boretti and Rosa (2019) exhibiting the projected utilization of water up to 2050, based on number of drivers of change, i.e. population/economic/technological growth and utilization pattern, indicate that the global water consumption will be 20–30% greater in 2050 than at present, driven primarily by demand for water. Industry is the big sector everywhere around the world that consumes massive quantities of water since the overall water used in industry accounts about 20% of the total (Zhao et al. 2009; Thabet et al. 2021a, b). Textile industry is gaining a great concern since it consumes vast amounts of water and their discharge is one of the main environmental impacts as the effluent containing dyes, colouring compounds and organic materials (Tayeb et al., 2019; Thabet et al. 2020; Ghaneian et al. 2008). Such heterogeneous discharge causes deterioration in the water bodies. Thus, the treatment of such effluents before its final disposal is imperative and gaining a concern for both industry and academia to meet the environmental regulations. However, colour removal from such discharge remains the major environmental concern since only 47% of dyestuffs used are biodegradable and the rest of them remain in the environment (Bia et al. 2009).

Up to now, various treatment schemes are introduced for dye removal including Biological (Tian and Yu 2020), chemical (Torrades and García-Montano 2014), and physical (Ashour and Tony 2020) techniques. However, chemical

✉ Maha A. Tony
dr.maha.tony@gmail.com

[1] Advanced Materials/Solar Energy and Environmental Sustainability (AMSEES) Laboratory, Basic Engineering Science Department, Faculty of Engineering, Menoufia University, Shebin El-Kom, Egypt

[2] Basic Engineering Science Department, Faculty of Engineering, Menoufia University, Shebin El-Kom, Egypt

treatments are the most efficient techniques, that is, adsorption (Ashour and Tony 2020a, b; Bayantong et al. 2021); catalytic oxidation (Tony and Lin 2021) and visible light-induced catalysis (Rezgui et al. 2021). Recently, Li et al. (2021a, b) applied nanoscale zero-valent iron for eliminating organic pollutants. Lui et al. (2021) and Fang and his co-workers (2021) introduced metal–organic framework as a water stable catalyst for removing organics, heavy metals and pharmaceuticals. More recently, Zou et al. (2022) introduced the aluminosilicate clay mineral-based composites as a photocatalysts for eliminating pollutants from aqueous stream.

Notably, advanced oxidation processes (AOPs) as chemical oxidation technology are gaining a considerable scientists' attention for reclaiming dye contaminating water since they are green choice, simple in operation and reliable for practical applications (Wang et al. 2021). The emerging field of AOPs is based on either heterogeneous or homogeneous mixture consisting of a strong oxidizing agent and transition metal. Although Fenton's reagent, which combines iron with H_2O_2, gained a vital role among the AOPs matrix for treating textile effluents; its practical applications are still limited. This is due to the significant challenge of the secondary waste collected after treatment (Rezgui et al. 2021). Hence, the determination of the appropriate catalyst is important to attain a considerable efficiency as well as minimizing the final waste. To date, most of the literature cited is based on applying iron-based salts as a source of Fenton' reagent.

Under the researchers' best policy scenario, achieving 'end-of-waste' status would be cleaner, inexpensive and superior solution equipped to fight the environmental damage (Li et al. 2011; Tony 2020a, b). In this regard, 'end-of-waste' photocatalysts by recovering catalyst materials can support the recycling of waste after wastewater treatment for beneficial use to avoid secondary waste materials without damaging human health and environment. Thus, the particularity of the current study is focused on the application of the superparamagnetic Mn–Zn ferrite as an alternative of classical iron source to be oxidized via H_2O_2 to treat textile dyed contaminated wastewater as an easy to recover novel photocatalyst.

Mn–Zn ferrites materials are technologically valuable since they posses high magnetic permeability (Rath et al. 1999), low core losses (Xuan et al. 2007) and they are thermally and chemically stable in aqueous systems (Garcia-Munoz et al. 2020). In adding up, the low band gap of Mn–Zn ferrite materials in comparison with anatase TiO_2 are attaining the advantage of being capable to absorb a part of visible light besides the UV light. That property allows them to display the energy positions of both valence and conduction bands (Yang et al. 2014; Garcia-Muñoz et al. 2020). Due to their elite properties, those materials are applied extensively in numerous fields such as electronic applications (Rath et al. 1999). Such characteristics are alarming them as suitable candidates for wastewater oxidation applications either by the generation of highly reactive hydroxyl (·OH) radicals, the reduction of protons and/or dioxygen into the superoxide radical. However, according to the authors' knowledge, there is a lack in literature for applying Mn–Zn ferrites as a source of superparamagnetic Fenton's photocatalyst. As previously stated in the literature (Vinosha and Das 2018), the magnetic catalysts posses the advantage of recoverable and recyclable materials for successive use.

Herein, the current investigation highlighted the application of the high magnetic behaviour, $Mn_{0.6}Zn_{0.4}Fe_2O_4$ nanoparticles as a photocatalyst for dye polluted wastewater oxidation as an easy recoverable catalyst. In the light of the dependence of magnetic properties with Mn and Zn ions concentrations variations, the composition $Mn_{0.6}Zn_{0.4}Fe_2O_4$ was selected at which the maximum magnetization is given. As well known, as the magnetization value of the magnetic nanoparticles is higher as the collecting process of them is easier. Nanoparticle was synthesized by an economically reliable co-precipitation technique and their catalytic activity for successive use is studied to confirm their novelty as a superparamagnetic photocatalyst for sustainability use. This in turn diverts waste after wastewater remediation from disposal, keeping it in the economy as a resource, which can reduce the environmental impacts arising from waste management.

Experimental section

Synthesis of Mn–Zn–Fe_2O_4 nanostructures

Nanosized $Mn_{0.6}Zn_{0.4}Fe_2O_4$ particles have been synthesized via the common co-precipitation synthesis routes as a fast simple technique using mild temperature range (Vinosha and Das 2018). The required metal reagents masses are attained according to the following reaction relation (Xuan et al. 2007):

$$(1-x)Mn^{2+} + xZn^{2+} + 2Fe^{3+} + 8OH^- \rightarrow Mn_{(1-x)}Zn_x(Fe_2O_4) + 4H_2O \quad (1)$$

where x is representing the molar percent ($0 < x < 1$). The precursors used during the current co-precipitation reaction are $Fe_2(SO_4)_3$, $ZnSO_4$ and $MnSO_4$ and all of them are used as received from the supplier (Sigma-Aldrich) without any further refinement. Thus, following the molar contents of ferrite material $Mn_{1-x}Zn_xFe_2O_4$, the stoichiometric compositions of precursors are calculated and the essential fractions were added then the solution was magnetically stirred to achieve homogeneity. Aqueous NaOH was used to adjust the pH value. Afterwards, the precipitated solution was continuously stirred under heating (80 °C) to obtain a thick precipitate. Thereafter, the as-synthesized nanoparticles were

subjected for successive washing using distilled water. As the result, $Mn_{0.6}Zn_{0.4}Fe_2O_4$ nanoparticles were obtained and characterized.

Characterization of the prepared nanosized $Mn_{0.6}Zn_{0.4}Fe_2O_4$

The composition, microstructure and sizes of the synthesized Mn–Zn ferrites are analysed. The phase structure of the prepared samples characterized by X-ray powder diffractometry XRPhillips X'pert (MPD3040) diffractometer with Cu-Kα radiation at room temperature. Furthermore, the particle size and morphology of the synthesized $Mn_{0.6}Zn_{0.4}Fe_2O_4$ nanoparticles investigated using HR-TEM (type Tecnai G20, FEI). Additionally, hysteresis loop was traced at 300 K using Lake Shore Cryotronics Model 7410 Vibrating Sample Magnetometer (VSM).

Synozol blue wastewater and photocatalytic oxidation

Synozol Blue CA (Reactive Blue 19) is used as a reactive dye source for preparing the synthetic textile wastewater solution, which supplied by DyStar Ltd., German, and used without further purification. Firstly, a 1000-ppm aqueous stock dye solution was prepared and the solution was further diluted as required. The as-synthesized $Mn_{0.6}Zn_{0.4}Fe_2O_4$ was used as the catalyst source of Fenton reaction and hydrogen peroxide (30% w/v) was used to initiate the Fenton's reagent reaction. The pH value of the synthetic wastewater solution was adjusted to the desired values, if needed, by using diluted sulphuric acid or sodium hydroxide. All chemicals were supplied by Sigma-Aldrich and used as received without further treatment.

100-mL dye-containing solution was added into a glass container; then, the Fenton reagent at specific concentrations was added after pH adjustment in order to demonstrate the effect of heterogeneous Fenton reaction. Thereafter, the solution was subjected to a magnetic stirring to ensure mixing and dispersion before exposed to a UV illumination of 253.7 nm (15 W-UV lamp, 230 V/50 Hz) by immersing the sleeved UV lamp inside a glass container containing the solution. Aliquot samples afterwards were withdrawn periodically at different time intervals for analysis. The graphical presentation of the experimental procedures is illustrated in Fig. 1.

Analysis

A UV–vis spectrophotometer, Unico UV-2100 model, USA, was used to investigate the residual Synozol Blue dye concentration corresponding to the maximum wavelength of 590 nm at set time intervals. Additionally, chemical oxygen demand (COD) of the treated samples was analysed using Lovibond Checkit direct COD Photometer, Germany. Prior to the samples subjected for measurements, the nanoparticles were separated using a micro-filter. The

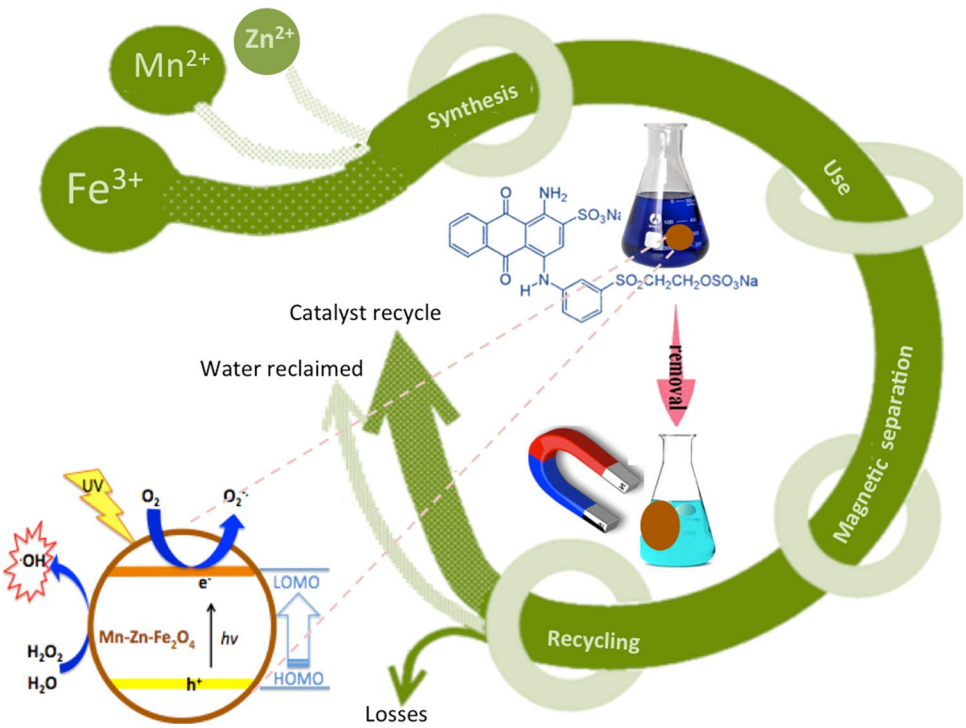

Fig. 1 Schematic illustration of experimental procedure

Table 1 Experimental range and levels of the independent factors of central composite design for Synozol Blue oxidation*

Factors	Original factors (τ)	Coded Factors (Γ)				
		$-\alpha$	-1	0	$+1$	$+\alpha$
Catalyst/mg L^{-1}	τ_1	25.879	30	40	50	54.121
H_2O_2/mg L^{-1}	τ_2	200.597	300	400	500	541.21

*$\alpha = 1.4121$; Coded factor = (original factor – its 0 level)/gap

Table 2 Experimental central composite design matrix of Synozol dye oxidation

Set No.	Factors			
	Codified factors		Original factors	
	Γ_1	Γ_2	τ_1	τ_2
1	−1	−1	30	300
2	−1	1	30	500
3	1	−1	50	300
4	1	1	50	500
5	−1.41421	0	25.879	400
6	1.41421	0	54.121	400
7	0	−1.41421	40	200.597
8	0	1.41421	40	541.21
9	0	0	40	400
10	0	0	40	400
11	0	0	40	400
12	0	0	40	400
13	0	0	40	400

samples' pH value was adjusted, if needed, using a digital pH meter model, AD1030, Adwa instrument, Hungary.

Central composite design model

Statistical tool based on response surface methodology, RSM, is applied for optimizing the experimental variables. Central composite experimental design (CCD) is chosen as a statistical technique. Such one is based on a multivariate nonlinear model for optimizing the response surface. That response influencing the various variables as well as categorizing the correlation between the controllable variables and the attained responses. In the current study, the influence of the most affecting parameters in the Fenton reaction, i.e. catalyst dose and hydrogen peroxide concentration was chosen to investigate their influencing on colour (ξ_1) and COD (ξ_2) removals' efficiency of Synozol Blue dye from aqueous matrix. Four levels were chosen for each of the two variables: catalyst (τ_1) and H_2O_2 (τ_2) as tabulated in Table 1 in their original and coded values.

The full factorial CCD experimental design for fitting the second-order polynomial model that requires only a minimum number of experiments is given in Table 2. Generally, the optimization technique including main steps, firstly:

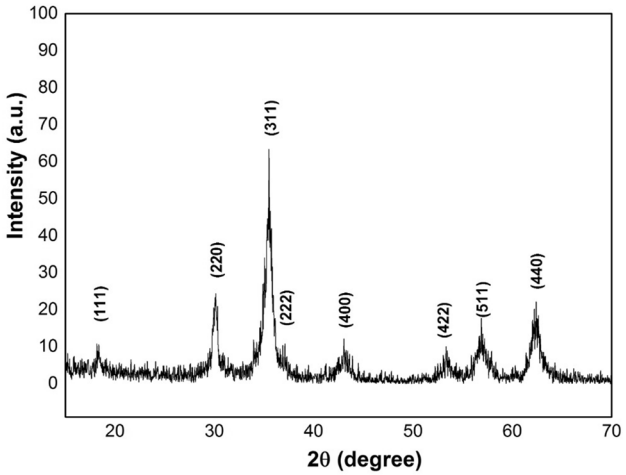

Fig. 2 XRD of the synthesized $Mn_{0.6}Zn_{0.4}Fe_2O_4$ nanopowder with M_H loop as an inset

conducting the statistically designed experiments (Table 2), followed by the estimation of the coefficients in a mathematical model, and finally predicting the response and checking the adequacy of the model. An empirical model was developed to correlate the response to the dye removal process that is based on second-order quadratic model as given by Eq. (2) to interact the interaction variables.

$$\xi_i = \beta_o + \sum \beta_i \Gamma_i + \sum \beta_{ii} \Gamma_i^2 + \sum \beta_{ij} \Gamma_i \Gamma_j \quad (2)$$

where ξ_i is the colour and COD removal responses; β_o, β_i, β_{ii} and β_{ij} are the model coefficient of the linear effect and double interactions; Γ_i and Γ_i^2 are the independent variables.

Results and discussions

Structural, magnetic and morphological characterization

X-ray diffraction pattern (XRD) of the prepared $Mn_{0.6}Zn_{0.4}Fe_2O_4$ nanoparticles ferrites is shown in Fig. 2. The obtained XRD reveals that the powder is crystallized in a single cubic spinel phase with definite crystalline planes reported on each peak in the figure.

Transmission electron micrographs, TEM, were performed for the prepared $Mn_{0.6}Zn_{0.4}Fe_2O_4$ ferrites nanoparticles and they are illustrated in Fig. 3 with their corresponding histogram. The micrographs reveal that the obtained particles are almost spherical in shape with nanosize ranges from 3 to 47 nm with most abundance particle size (MAPS) about 15.12 nm. It is also obvious that small number of agglomerated particles is existed together with the separated ones in the obtained powder. The agglomeration can be referred to Van der Walls or electrostatic forces between particles (Eltabey et al. 2017). As a direct proves for the obtained powder has superparamagnetic behaviour, the hysteresis loop (M-H loop) at room temperature was measured and it is illustrated as inset in Fig. 1. The obtained loop is closed one with no coercivity that is considered to be a typical superparamagnetic behaviour.

Effect of different treatment systems on reaction time

Catalytic oxidation of Synozol Blue CA dye for its removal from aqueous solution has been investigated. In this light, the effects of reaction time on $Mn_{0.6}Zn_{0.4}Fe_2O_4/H_2O_2$; $Mn_{0.6}Zn_{0.4}Fe_2O_4/H_2O_2$/UV and H_2O_2/UV oxidation systems were examined to investigate an experimental condition for further research. The efficacy of those techniques was tested in the terms of color and COD removals. Thus, firstly, the as-prepared $Mn_{0.6}Zn_{0.4}Fe_2O_4$ was added to the wastewater at either its natural pH value (6.8) or pH 3.0 and thereafter the reaction was initiated by adding 400 mg L^{-1} of H_2O_2 for oxidizing Synozol Blue dye using Dark Fenton test. The results displayed in Fig. 4a and b demonstrate that both colour and COD removal are higher when the pH value of wastewater is adjusted at 3.0. The dye removal efficiency reached to only 18% and 1% for colour and COD removals, respectively, using the wastewater without pH control in comparison to 44 and 27% for colour and COD removals, respectively, when adjusting the wastewater's pH at 3.0. Therefore, in the other set of experiments, wastewater was adjusted at 3.0 to conduct Fenton's reaction. Thus, photo-Fenton's reaction, $Mn_{0.6}Zn_{0.4}Fe_2O_4/H_2O_2$/UV, using 40 and 400 mg L^{-1} applied under UV illumination and the removal efficiency reached to 76 and 58% for colour and COD removals, respectively. Comparing the combined $Mn_{0.6}Zn_{0.4}Fe_2O_4/H_2O_2$ system with the solo hydrogen peroxide system, under

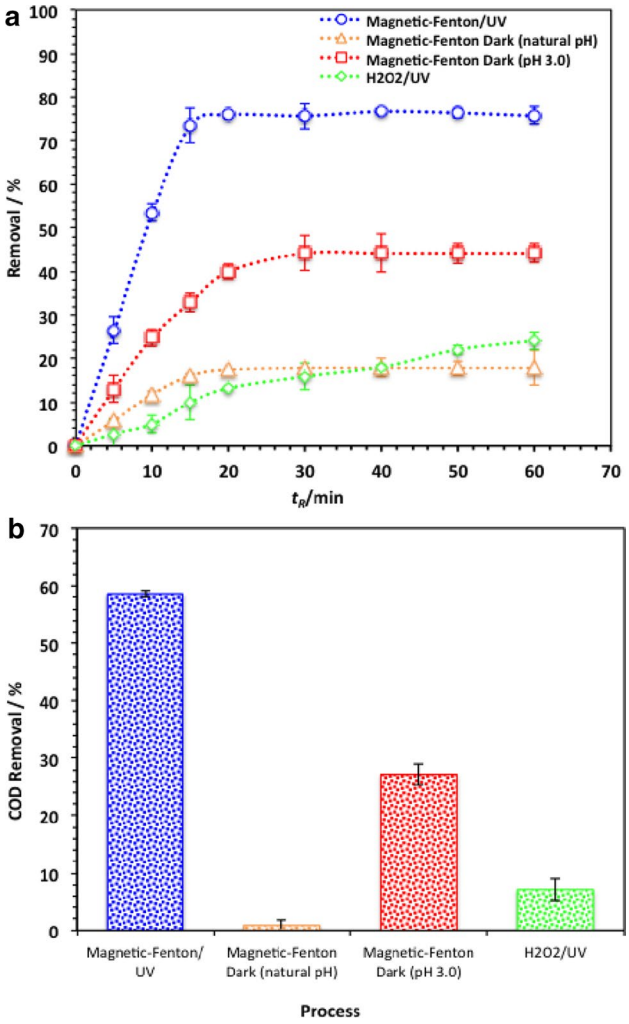

Fig. 4 Effect of different treatment systems on Synozol Blue removal (**a**) Colour removal; (**b**) COD removal

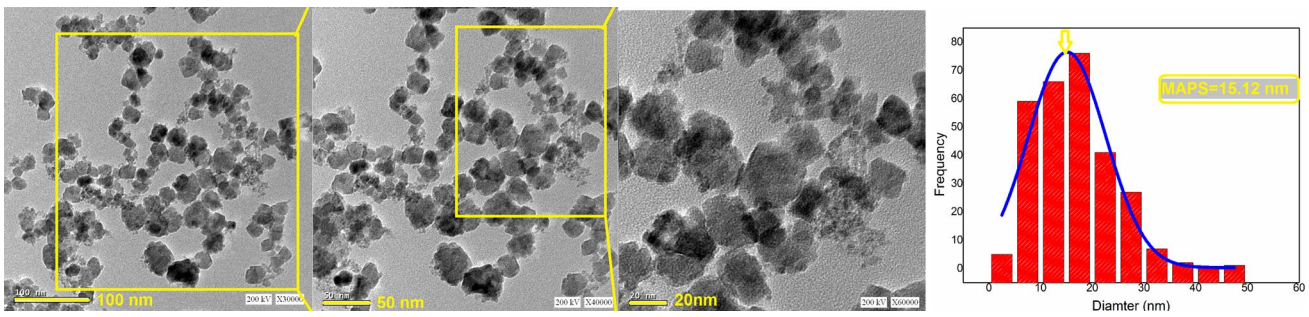

Fig. 3 TEM micrograph of the synthesized $Mn_{0.6}Zn_{0.4}Fe_2O_4$ nanopowder with particle size histogram

the UV illumination, the removal reached to 31 and 7% for colour and COD removals, respectively.

It is clear from comparing the results in Fig. 4a and b that the UV illumination is an effective tool for solo H_2O_2 oxidation or photo-Fenton reaction as the removal is much higher in comparison to the dark reaction test. It is noteworthy to mention that the photo-Fenton reaction is the most effective reaction for dye oxidation. Also, 15 min of reaction time is enough to attain such removals for the Fenton reaction time, t_R and after that time a plateau is attained in all Fenton combinations. But, with prolonging of oxidation time, the Synozol Blue dye removal slowed down and its removal efficiency became stabilized. However, 60 min time is needed for the solo hydrogen peroxide system to complete the reaction.

This rapid oxidation rate in the initial stage for all the Fenton systems and H_2O_2 oxidation is associated with the ˙OH radicals as the reaction intermediates. Such radicals are the main responsible of the dye oxidation. As the time exceeds, ˙OH radicals produced are declined. Besides, a reduction in the H_2O_2 amount is attained with the formation of other radicals that presents in the reaction medium and inhibits the oxidation rate. Furthermore, Fenton reaction is utilizing H_2O_2 reagent for activating the catalyst. However, such reagent, H_2O_2, is consumed after the initial oxidation period. Afterwards, more radicals are produced and the reaction becomes more complicated. The radicals generated in such case are so-called hydroperoxyl radicals, HO_2, which declines the overall oxidation rate with the time increase. Thus, those radicals inhibit the oxidation of Synozol dye rather than oxidizing them (He and Lei 2004).

In the solo H_2O_2 system, as the time proceeds, the peroxide is consumed and therefore, the dye oxidation rate is reduced. According to the previous investigations (Najjar et al. 2001; He and Lei 2004; Tony 2021a, b, c, d), numerous studies are dealing with the phenomenon of the oxidation rate that is higher at the initial reaction time and declines while the reaction proceeds. This is related to the ˙OH radicals' production that is too high at the first reaction stage. Although the same rapid initial dye oxidation tendency occurs in the initial stage of all the Fenton's systems, the removal is limited to only 18% for dye removal using Dark Fenton test. This is related to the presence of the UV illumination that initiating more ˙OH to produce and thus the oxidation rat is enhanced (Maroudas et al. 2021).

Effect of contaminant load

Fenton oxidation set was made at various initial dye concentrations ranged from 15 to 100 ppm in synthetic dye medium and the treatment data are displayed in Fig. 5a and b for colour and COD removals, respectively. From a quick scan of previous studies (Shanmugam et al. 2019; Tony and Lin 2020a; Abdollahzadeh et al. 2020), it was observed that oxidation rate is so far highly dependent on the initial pollutants load. Hence, in this regard, the effect of dye load is investigated at pH value 3.0 with 40 and 400 mg L^{-1} of catalyst and H_2O_2 concentrations, respectively. According to the experimental results in Fig. 5, the dye oxidation rate was found to be dependent on the initial dye concentration. A maximum of 96% dye oxidation could be achieved within 15 min Fenton's oxidation when 15 ppm of dye load is treated. However, the higher dye load is significant in making the process feasible for practical applications. Thus, higher dye loads are also investigated; however, the oxidation rate is declined with increasing the dye load. At a glance of Fig. 5a and b, the rate declined from 96 and 78% to 75–34% and 60–17% for colour and COD removals, respectively, for the gradual increase in the dye loads from 15 to 100 ppm.

The rate and efficacy of Synozol Blue dye oxidation decrease with increasing the initial dye load. This could be attributed to the increased concentration of the toxic dye in

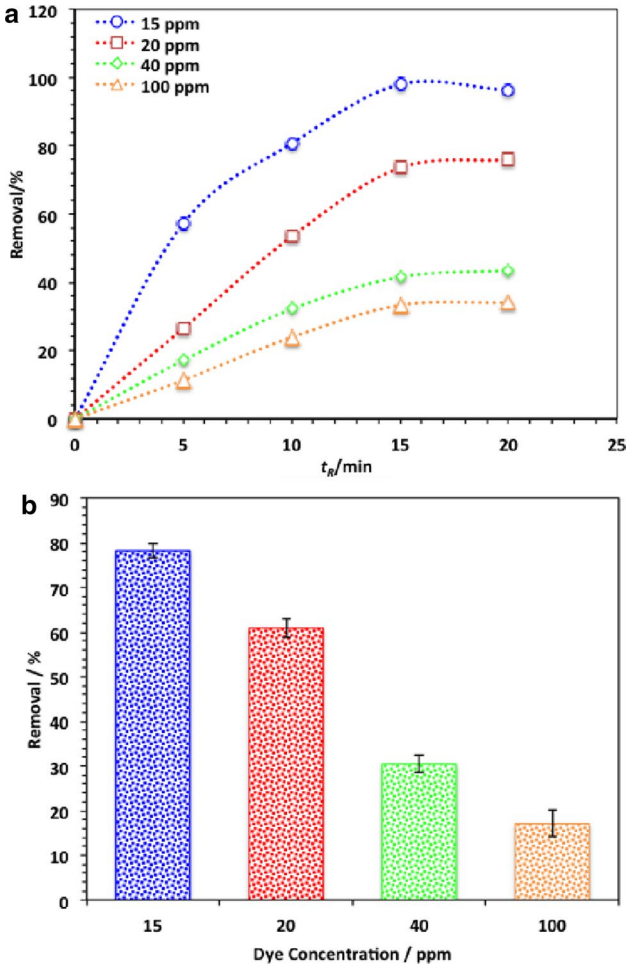

Fig. 5 The effect of Synozol Blue load on the $Mn_{0.6}Zn_{0.4}Fe_2O_4$/H_2O_2/UV oxidation (Catalyst 40 mg L^1, H_2O_2 400 mg L^{-1}, pH 3.0)

the reaction medium leads to a decrease in the ˙OH radicals, while the Fenton's reagent concentrations kept constant. Such explanation is in a good agreement with that earlier stated as the oxidation reaction is highly dependent on those radicals (Zafar et al. 2020; Tony 2021a, b, c, d). In addition, Shanmugam and his co-workers (2019) had been previously reported the same trend in treating acid blue 113 dye using Fenton's reagent.

Fenton's multiple parameters

Catalyst, H_2O_2 and pH value effect

Decomposition of H_2O_2 in the presence of a catalyst, $Mn_{0.6}Zn_{0.4}Fe_2O_4$, for generating hydroxyl radicals is essential for Fenton's reaction. However, it is crucial in keeping either H_2O_2 or catalyst concentrations minimal since the higher dosage declines the reaction efficiency. Thus, to examine the influence of Mn–Zn ferrites catalyst on the Fenton's oxidation of Synozol Blue CA dye, experiments were undertaken to determine the influence of catalyst dose on reaction kinetics.

Figure 6a and b illustrates the effective dye oxidation process by varying the concentration over the range of 20–80 mg L^{-1}. It is obvious that the oxidation efficiency increases from 51 to 72% when the superparamagnetic $Mn_{0.6}Zn_{0.4}Fe_2O_4$ catalyst concentration increases from 10 to 20 mg L^{-1}. Additionally, further catalyst increase to 40 mg L^{-1} results in higher removal efficiency reaches to 96%. With a further increase in catalyst more than to 40 mg L^{-1}, a marginal decrease in the removal rate to 87% is attained. The same trend is observed for the COD reduction efficiency.

Mn, Zn and iron ions are critical for creating the photoactive hydroxo-complexes, which absorb the photons in the UV illumination and then generate the (·OH) radicals. The metal ions are formed and react with H_2O_2 to form further ·OH radicals and metal ions again. Synozol dye contains aromatic structures, ·OH attack the aromatic rings in the dye molecules, then get hydroxylated and build up a hydroycyclohexadienyl radical as a result from the ·OH attack on the aromatic ring. The overall reaction is strongly oxidizing the dye molecules (Chen and Pignatello 1997).

Figure 6c and d displays the effects of the increase in H_2O_2 concentration on Synozol Blue oxidation rate while all other parameters are kept constant (catalyst 40 mg L^{-1} and pH 3.0). The results demonstrate that there is an increase in the dye removal rate (96 and 73% for colour and COD, respectively) with the peroxide increase. Moreover, the results showed that 400 mg L^{-1} is recorded the optimal peroxide dose. Such investigation correlates with previous investigation by the author (Tony 2020a). At excess H_2O_2 dosage more than the optimal dose, H_2O_2 itself would act as hydroxyl radical scavenger than a producer. Hence, the result is a terminal effect on the dye removal (71% for 800 mg L^{-1} H_2O_2 addition). This observation was previously remarked by Rezgui et al. (2021).

According to the previous studies (Shanmugam et al. 2019; Rezgui et al. 2021), Fenton reaction is so sensitive to the pH value of the aqueous media. Figure 6e and f displays that the decrease in the pH value is corresponding to a high colour and COD removal efficiency. This fact illustrates that the Fenton reaction is more active in the acidic range, while in alkaline conditions; hydrogen peroxide oxidizes itself into H_2O and O_2 that renders the oxidation reaction (Shanmugam et al. 2019). Therefore, the pH of the wastewater was kept in the acidic range by manual addition of sulphuric acid for oxidizing via Fenton reagent.

Oxidation mechanism

Under the UV illumination, $Mn_{0.6}Zn_{0.4}Fe_2O_4$ was irradiated, and an electron (e)/hole (h) pair was generated on its surface according to Eq. (3). This photo-induced hole could react with water (H_2O) or may be hydroxyl ion (OH) to produce hydroxyl radicals (˙OH) (as seen in Eq. (4 and 5). Also, the photo-induced electron could be captured via the hydrogen peroxide reagent and then ˙OH radicals are produced. Such reaction may limit the recombination of holes and electrons and hence improving the catalytic activity of the catalyst. Additionally, H_2O_2 will react with Fe^{3+} and Fe^{2+} to activate the Fenton reaction that generating more hydroxyl radicals (Eq. 6, 7). Thus, hydroxyl radicals are produced through different pathways, and an enhancement in the rate of oxidation was observed (Ramirez et al 2007; Sharma et al. 2015).

$$Mn_{0.6}Zn_{0.4}Fe_2O_4 + h\nu \rightarrow Mn_{0.6}Zn_{0.4}Fe_2O_4\left(e^-_{CB} + h^+_{VB}\right) \quad (3)$$

$$h^+_{VB} + H_2O \rightarrow H^+ + OH^{\cdot} \quad (4)$$

$$h^+_{VB} + H^- \rightarrow OH^{\cdot} \quad (5)$$

$$Fe^{3+} + H_2O_2 \rightarrow Fe^{2+} + HOO^{\cdot} + H^+ \quad (6)$$

$$Fe^{2+} + H_2O_2 \rightarrow Fe^{3+} + OH^- + OH^{\cdot} \quad (7)$$

H_2O_2 promotes the reaction medium with ˙OH radicals after initiation with UV illumination according to Eq. (8). However, higher doses of such reagent more than the optimal concentration inhibit the oxidation rate since the peroxide competing the pollutants for reacting with the ˙OH radicals (Eq. 9) (Neamtu et al. 2002). Also, recombination reaction of •OH radicals and likewise •OH radical is further scavenging the overall radicals produced (Eq. 10, 11) (Tamimi et al. 2008). Such generated ˙OH radicals attacking the Synozol

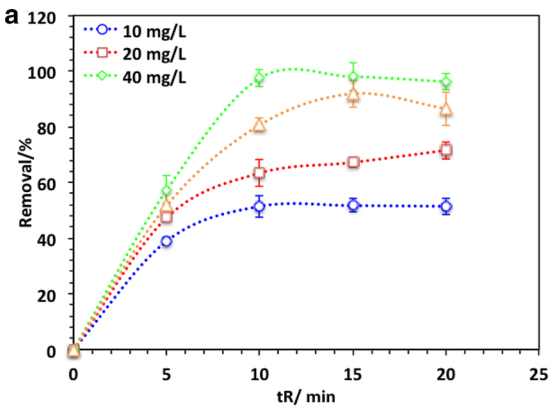
a
10 mg/L
20 mg/L
40 mg/L
Removal/%
tR/ min

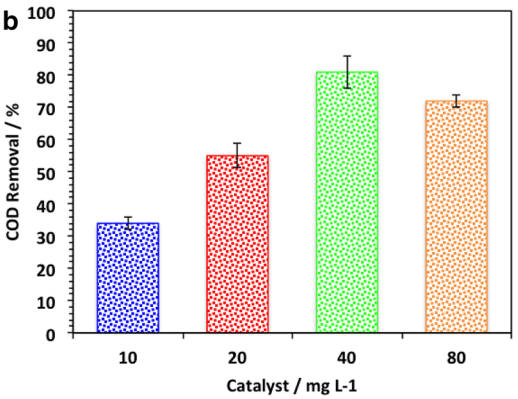
b
COD Removal / %
Catalyst / mg L-1

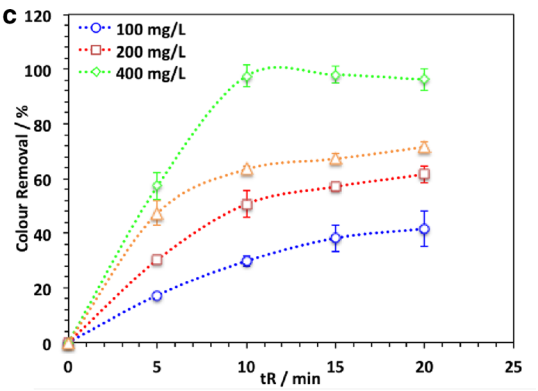
c
100 mg/L
200 mg/L
400 mg/L
Colour Removal / %
tR / min

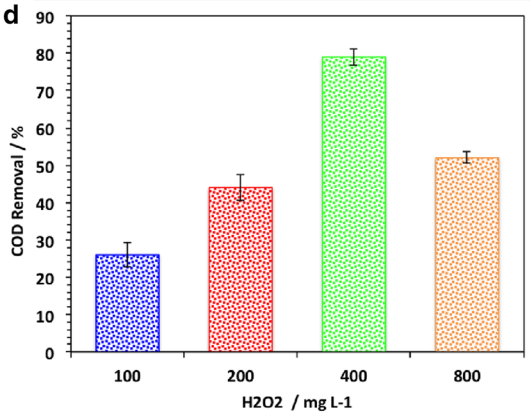
d
COD Removal / %
H2O2 / mg L-1

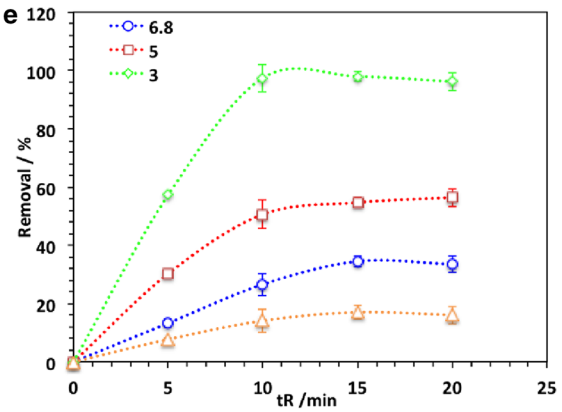
e
6.8
5
3
Removal / %
tR /min

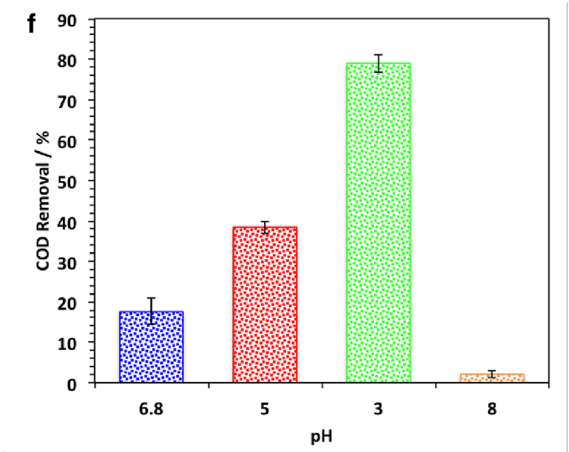
f
COD Removal / %
pH

◂**Fig. 6** Effect of operating parameters on $Mn_{0.6}Zn_{0.4}Fe_2O_4/H_2O_2$/UV system: Effect of catalyst (H_2O_2 400 mg L^{-1}, pH 3.0) on (**a**) colour and (**b**) COD removals; Effect of H_2O_2 (Catalyst 40 mg L^1, pH 3.0) on (**a**) colour and (**b**) COD removals; (**c**) Effect of pH (Catalyst 40 mg L^1, H_2O_2 400 mg L^{-1}) on (**a**) colour and (**b**) COD removals

dye molecules that consists of aromatic structures to get them hydroxylated and build up a hydroycyclohexadienyl radical as seen in Eq. (12).

$$H_2O_2 + h\nu \rightarrow 2^{\cdot}OH \tag{8}$$

$$H_2O_2 + HO^{\cdot} \rightarrow HO_2^{\cdot} + H_2O \tag{9}$$

$$HO_2^{\cdot} + OH^{\cdot} \rightarrow H_2O + O_2 \tag{10}$$

$$OH^{\cdot} + OH^{\cdot} \rightarrow H_2O_2 \tag{11}$$

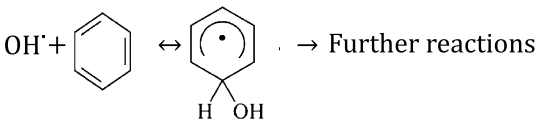

(12)

The ability of hybrid combined metal nanoparticles to absorb light as a photocatalyst affecting the pollutants oxidation. Combining Mn with ZnO in ferrite molecule explains the high performance of such photocatalyst in the visible light-driven band. The photoelectrons transferred in the catalyst surface and thus $^{\cdot}O_2$ radicals is formed via the reaction with the solvated oxygen. In the other route, the left H^+ in the valence band may additionally react with H_2O to form hydroxyl radical, which then could together with $^{\cdot}O_2$ may oxidize the organics. Therefore, via such mechanism, the electron–hole pairs are more effective and their lifetime is prolonged (Thakur et al. 2020; Abdel Maksoud et al. 2020; Li et al. 2021a, b; Fang et al. 2021). Moreover, the active ·OH radicals generated through the reaction attack the aromatic structure contained on the dye molecules to hydroxylate it by forming intermediate radicals to finally mineralize the dye molecules (Chen and Pignatello 1997; Thabet et al. 2021a).

Comparison of the Synozol dye treatment technologies using the superparamagnetic modified Fenton type reaction ($Mn_{0.6}Zn_{0.4}Fe_2O_4$/ H_2O_2/UV) from the current study with those from previous studies, which are stated in the literature, is tabulated in Table 3. It could be concluded that $Mn_{0.6}Zn_{0.4}Fe_2O_4/H_2O_2$/UV oxidation attained an efficient superior treatment for Synozol dye removal (96%) in comparison to other used systems. Although Fenton treatment is a dual treatment system from a combination of a catalyst and a H_2O_2 compared to other treatment systems reported in Table 3, such systems exhibited some drawbacks. Such drawbacks including the long reaction time, the need of biomass and quantities of chemical agents are not recorded in the current Fenton system. Thus, the end products from such treatments in comparison to Fenton system are the formation of toxic end products. Also, the other treatments' cost is expensive compared to the Fenton's cost. Besides, the use of the physicochemical treatments, i.e. adsorption treatment, the result is the formation of secondary effluents, which may need further treatments since they could not mineralize the pollutants. Hence, such groups of disadvantages are not related to the current Fenton system besides Fenton's reagent is an environmentally friendly technique compared to that listed in Table 3. Therefore, this is recommending such technology for reactive dye removals.

Experimental design and optimization

The effect of the two independent critical parameters, i.e. catalyst and H_2O_2 concentrations on the Fenton oxidation of Synozol dye was simulated using central composite experimental design (Table 2). The quadratic polynomial model equation form validates the associated response functions colour removal ($\%\xi_1$) and COD removal ($\%\xi_2$) as follows (SAS 1990):

$$\xi_1(\%) = 95.40 - 4.22\Gamma_1 + 1.34\Gamma_2 - 15.51\Gamma_1^2 + 2.00\Gamma_1\Gamma_2 - 13.26\Gamma_2^2 \tag{13}$$

$$\xi_2(\%) = 89.60 - 3.92\Gamma_1 + 1.114\Gamma_2 - 14.61\Gamma_1^2 + 1.75\Gamma_1\Gamma_2 - 13.11\Gamma_2^2 \tag{14}$$

Fisher's statistical test (*F*-test) for analysis of variance (ANOVA analysis) (Table 4) was performed to investigate the statistical significance and the suitability of the proposed quadratic model. Generally, the model is recognized to be the best fit with a low standard deviation, a small probability value ($Pr < 0.005$) and a high regression coefficient (r^2) (SAS, 1990). As seen from Table 5, r^2 for the oxidation reaction is high for the two models with a low probability (*Pr*) value of 0.0001. Additionally, a good correlation between the predicted and experimental values of the quadratic model was attained for the two models as given in Fig. 7a and b.

The experimental parameters effects on the examined responses are presented graphically in Fig. 7 (c, d) that illustrates the response of each experimental variable and the major interactions between those variables. Examination of the 3-D surface graphs and contour plots in Fig. 7c and d illustrates that the colour and COD removals increase with increasing the concentrations of both $Mn_{0.6}Zn_{0.4}Fe_2O_4$ and H_2O_2. However, the curvature of the 3-D surface shown in Fig. 7c and d reveals that there is an interaction effect between catalyst and H_2O_2 doses. Such interaction supports the formation of hydroxyl radical intermediates that positively oxidizing the Synozol Blue molecules and mineralizing them. However, a further

Table 3 Comparison of different treatment methodologies for Synozol dye contaminated wastewater matrix*

Treatment process	Synozol Dye (colour index)	Operating conditions					Removal/%	Ref.
		Catalyst/mg L^{-1}	H_2O_2/mg L^{-1}	pH	T/°C	t_R		
$Mn_{0.6}Zn_{0.4}Fe_2O_4$ *np* / H_2O_2/UV	Synozol Blue (Reactive Dye 19)	Mn-Zn Ferrites, 40	400	3.0	26 °C	15	96%	Current work
UV/$K_2S_2O_8$ Process	Synozol Blue (Reactive blue 19)	$K_2S_2O_8$, 1.4	–	3.0	NA	180	78%	Rezaee et al. 2008
SiO_2 *np*	Synozol Blue (Reactive blue 19)	SiO_2, 750	–	5.0	30 °C	90	95%	Toosi et al. 2017
Sulfur-doped TiO_2 (S-TiO_2) *np* /US	Synozol Blue (Reactive blue 19)	S-TiO_2, 50		3.0	25 °C	120	90%	Khan et al. 2015
Electrocoagulation (10 Volt)	Synozol Blue (Reactive blue 19)	Iron electrodes	–	9.0	Room T	25	86%	Khedher et al., 2017
Biological treatment	Synozol Red K-4B	Candida tropicalis 4S		7.0	30 °C	21 days	93%	Ilyas et al. 2015
Biological treatment	Synozol Red HF-6BN (Reactive Red 195)	Aspergillus niger & Nigrospora sp.	–	6.0	40–50 °C	24 days	96%	Ilyas and Rehman 2013
Aerobic granules treatment	Synozol Red K-4B	Microbial granular sludge	–	NA	NA	66 days	62%	Muda et al. 2010

*np: nanoparticles; NA: not available; US: ultrasonic

Table 4 ANOVA for the regression model and the respective models terms*

Source	DF	SS	MS	F	Pr > F	r^2	Adj- r^2
ξ_1							
Model	5	2741.126	548.2252	71.53899	0.0001	98.08%	96.71%
Error	7	53.64315	7.663307				
Total	12	2794.769					
ξ_2							
Model	5	2519.431	503.8861	84.38274	0.0001	98.37%	97.20%
Error	7	41.80005	5.971436				
Total	12	2561.231					

DF: Degree of freedom; SS: Sum of Squares; MS: Mean Squares; F-value) Fisher test; Pr: Probability

Table 5 Photocatalytic kinetic models and statistical analysis of Synozol Blue oxidation via $Mn_{0.6}Zn_{0.4}Fe_2O_4/H_2O_2$/UV*

Kinetic model	Linear equation	Parameters	Values			
			T/°C			
			26ºC	40ºC	50ºC	60ºC
Zero-order	$C_t = C_o - k_Z t$	K_Z/min^{-1}	0.5319	0.5868	0.7115	0.7146
		$t_{0.5}$	14.41	13.06	10.77	10.72
		r^2	0.91	0.89	0.89	0.74
First-order		K_F (min^{-1})	0.2901	0.1625	0.0911	0.0746
	$C_t = C_o - e^{k_F t}$	$t_{0.5}$/min	9.29	7.61	4.26	2.39
		r^2	0.91	0.97	0.99	0.99
Second-order	$\left(\frac{1}{C_t}\right) = \left(\frac{1}{C_0}\right) - k_S t$	K_S/L mg^{-1} min^{-1}	0.2366	0.0444	0.0123	0.0088
		$t_{0.5}$/min	0.28	1.47	5.30	7.41
		r^2	0.88	0.79	0.94	0.94

*C_o and C_t: initial and at time t dye concentration (mg L^{-1}); t: time (min); k_Z, k_F, k_S: kinetic rate constants of zero-, first- and second-reaction kinetic models

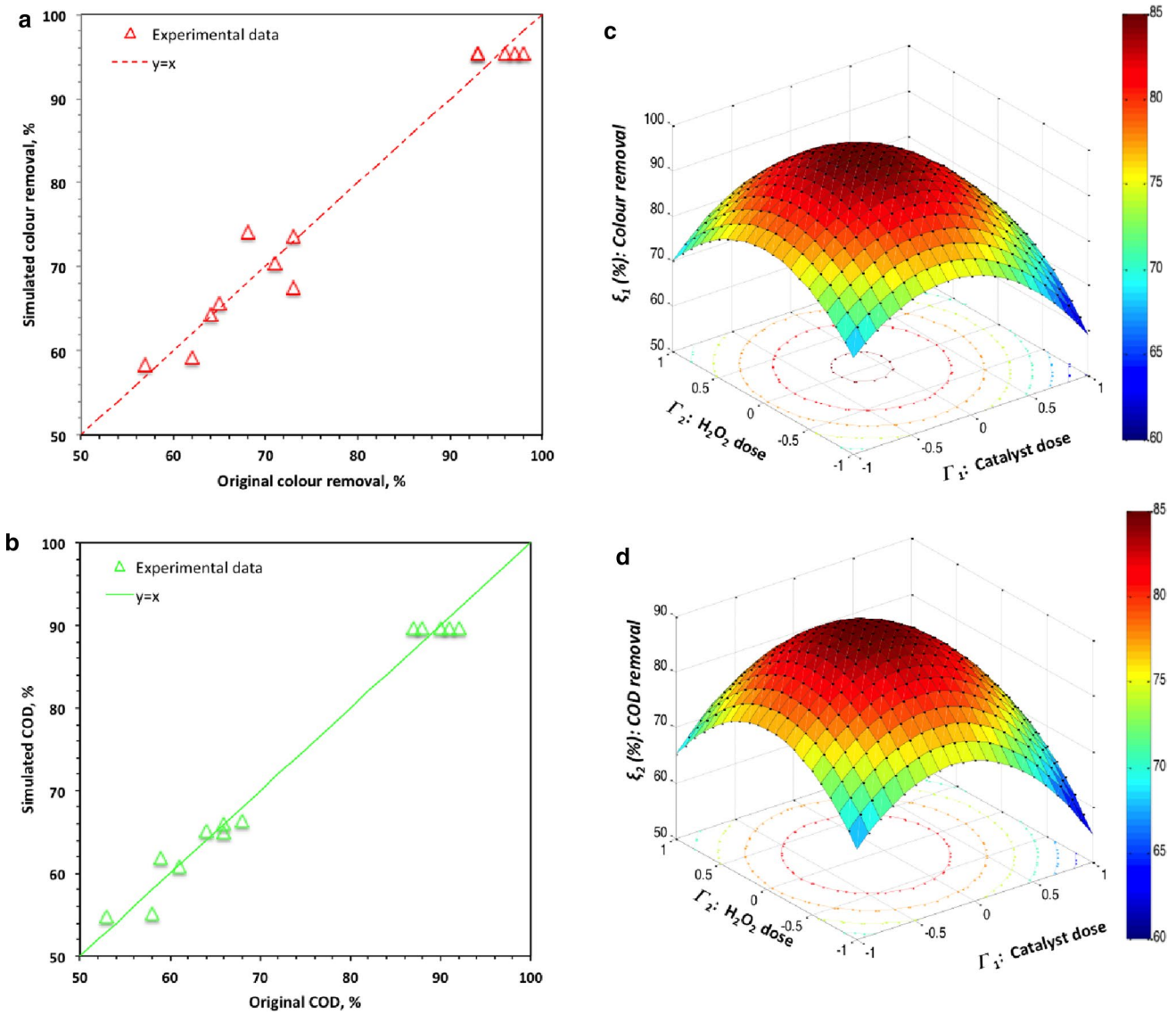

Fig. 7 Central composite design (CCD) optimization of $Mn_{0.6}Zn_{0.4}Fe_2O_4/H_2O_2/UV$ system: (**a**) Original and estimated ζ_1 response plot; (**b**) Original and estimated ζ_2 response plot; (**c**) 3-D surface and contour plot of ζ_1 model; (**d**) 3-D surface and contour plot of ζ_2 model; (**e**) Overlay contour plots for the optimal region of two responses (ζ_1, ζ_2); (**f**) Comparison of Synozol dye oxidation at manually optimized conditions and via CCD values

increase in the reagent doses results in a reduction in the dye removal rate. Thus, the optimal ratio of the catalyst/H_2O_2 is needed to maximize the hydroxyl radical production yield.

Also, a graphical optimization displayed in Fig. 7e locates that the area (lighter portion zone) of the optimal condition of Fenton reaction ($Mn_{0.6}Zn_{0.4}Fe_2O_4$ based system) for Synozol Blue CA dye oxidation. It can be seen that the optimal feasible response values are in the factors space. All the independent variables and their effective responses (colour and COD removals) with the particular high and low limits of the experimental region are significant and fit the standards.

To verify the validity of the proposed models, the statistically optimized values of the operating parameters attained from Mathematica software (V 5.2), for both catalyst and H_2O_2 were 39 and 404 mg L^{-1}, respectively, and additional three replicates of experiments were performed. The attained predicted removal values of colour and COD (which are presented in Fig. 7f and the inset) are compared with the manually optimized conditions. After 15-min of reaction time, the measured percentage of colour and COD removals attained as 98 and 87%, respectively, that is close to the predicted value (96 and 89%), using CCD. These results verify that the RSM based on CCD is adequate approach for optimizing the operating parameters influencing dye oxidation via

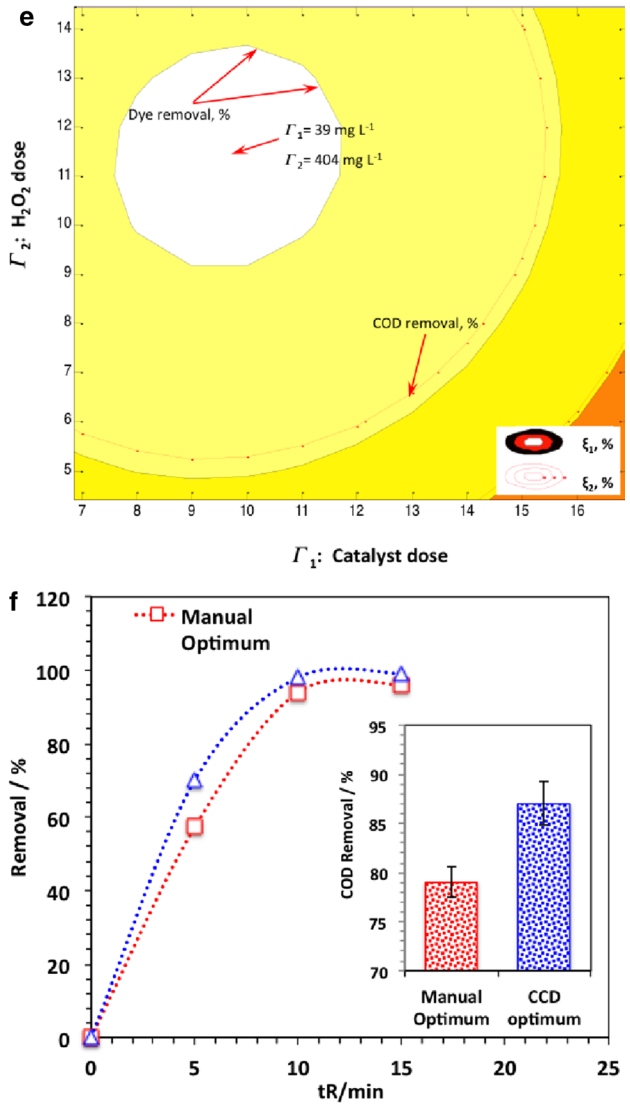

Fig. 7 (continued)

Fenton's reaction based on $Mn_{0.6}Zn_{0.4}Fe_2O_4$ nanoparticles as a superparamagnetic catalyst.

Continuous-flow performance

To further investigate the feasibility of treating Synozol Blue dye wastewater on a large scale, a continuous-flow laboratory-scale experiment was examined as an indication for practical application (Ashour and Tony 2017; Wang et al. 2021). A stock solution of Synozol Blue dye wastewater was pumped at various volumetric flow rates at a steady rate to a container under the UV reactor that is the same as in the batch experiment and stirred with a magnetic stirrer.

The essential parameter examined in this series of experiments was the effect of the hydraulic retention time, *HRT*, in the UV illumination reactor on the degree of oxidation of the Synozol Blue in wastewater as illustrated by the following relationship: $\boldsymbol{HRT} = \frac{V}{Q}$, where V is the volume of the wastewater in litre and Q is the volumetric flow rate in L min^{-1}. The results displayed in Fig. 8 illustrate the rate of the dye oxidation for the continuous process operating at various *HRTs*. The data showed that, following the initial period of each experiment, there was a transient phase during which the dye oxidation rate evaluated by the colour removal rates is increased, followed by a steady state removal rate. This is in accordance with the might reasonably be estimated, the high *HRT* attain an increase in stabilization of the effluent and vice versa. Such results are in agreement with the previously reported in the literature (Zou et al. 2020) that treated pharmaceuticals contaminated wastewater with such Fenton's reagent.

Temperature effect on kinetics and thermodynamics

Temperature is an energetic influencing factor on the oxidation reactions since it affects the reaction rates. To examine its influence on the reaction, experiments over a temperature range of 26 -60ºC were conducted. The data in Fig. 9a and b revealed that a decrease in reactive dye removal efficiency from 96 to 67% and from 78 to 49% for colour and COD removals, respectively, through the temperature increase in the studied range. This may be attributed to, at high temperatures; H_2O_2 decomposes into O_2 and H_2O rather than the formation of the highly reactive hydroxyl radicals. Thus, H_2O_2 reagent role becomes a free radical scavenger rather than a producer, which reduces the oxidation reaction. Previous work reported similar reaction trend in treating organic loaded wastewater via Fenton' s reaction (Guede et al. 2003).

Temperature's influence on Synozol Blue oxidation also was evaluated by kinetic and thermodynamic parameters. Kinetic parameters were obtained by applying the linearized form of zero-, first- and second-order kinetic models, to give estimation for the reactor design and system control that highlighting the treatment cost for both capital and operating expenses (Al Momani et al. 2008; Tony 2021a). Table 5 displays the estimated zero-, first- and second-order kinetic models. Examination of the regression coefficient (r^2) values shows that the highest values are corresponding to the first-order kinetic model. Thus, this verified the first-order is the best fit of the experimental results of Synozol oxidation through the modified Fenton's type reaction. As tabulated in Table 5, the first-order model rate constants (k_F) are decreased from 0.2901 to 0.0746 L mg^{-1} min^{-1} as the temperature increasing from 26 to 60 °C. Also, the corresponding half-reaction time ($t_{0.5}$) are decreased with increasing the temperature. This examination is in agreement with the previously recommended in the literature (Pintor et al. 2011; Ioannou and Fatta-Kassinos 2013) as they suggested

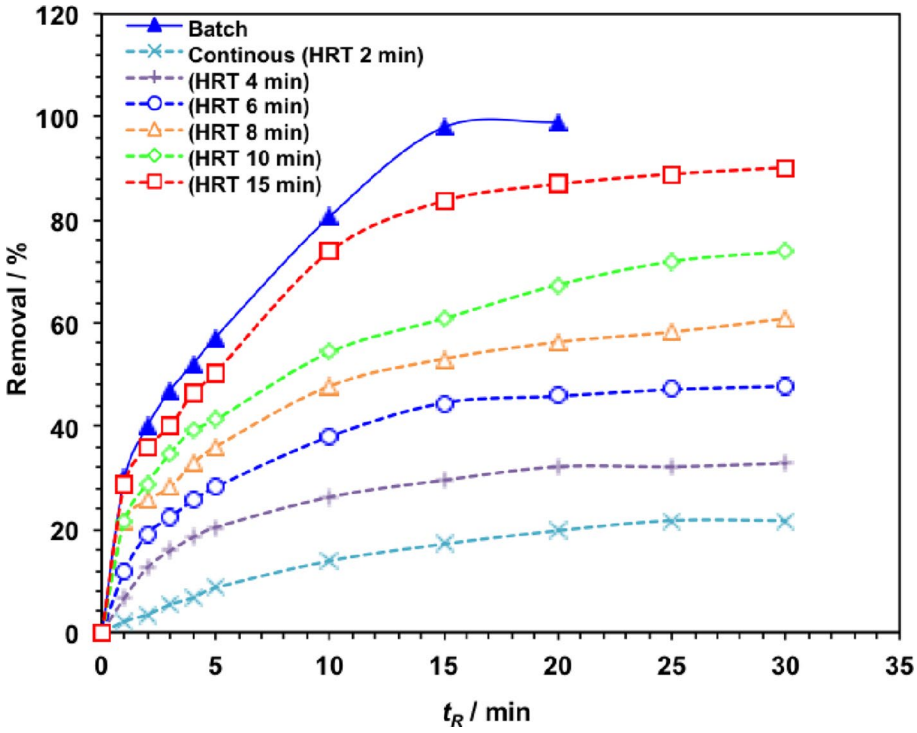

Fig. 8 Synozol Blue dye oxidation with the reaction time for the continuous $Mn_{0.6}Zn_{0.4}Fe_2O_4/H_2O_2$/UV system (Catalyst 40 mg L^1, H_2O_2 400 mg L^{-1}, pH 3.0)

the maximal Fenton's reaction yield is attained within the temperature range of 17–38 °C.

To further explore the temperature effect on the oxidation process of Synozol Blue, the thermodynamic activation parameters were obtained by the Arrhenius equation that is based on the first-order kinetic model ($\ln k_F = \ln A - \frac{E_a}{RT}$), where A is the pre-exponential factor constant; Ea is the energy of activation (kJ mol^{-1}); R is the gas constant (8.314 J mol^{-1} K^{-1}) and T is temperature (K). The linear plot of ln k_F versus 1/T gives a relationship whose slope is corresponding to ($-Ea/R$) that could be used to calculate Ea (Fig. 10). The thermodynamic activation parameters of the oxidation are evaluated by the Eyring equation ($k_F = \frac{k_B T}{h} e^{\left(-\frac{\Delta G^\circ}{RT}\right)}$), where k_B and h are Boltzmann and Planck's constants, respectively. Thus, the enthalpy (ΔH^o) and the entropy (ΔS^o) of activation could be calculated from the relation of $\Delta H^\circ = E_a - RT$ and $\Delta S^\circ = \left(\Delta H^\circ - \Delta G^\circ\right)/T$, respectively (Ahmadi et al. 2016). The results attained from such relations are displayed in Table 6 indicated that the non-spontaneously of the oxidation process since $\Delta G^o > 0$ and the degree of non-spontaneity increases as the temperature increases. With the positive ΔH^o values, the endothermic oxidation reaction nature is verified. Also, the negative ΔS^o values confirm the non-spontaneous nature of the oxidation process which exhibited a decrease in the degree of freedom of the dye molecules and maintained a high radicals species, ·OH, yield. Previous work by Argun and Karatas (2011) reported the endothermic Fenton oxidation process. Additionally, Pourali et al. (2020) highlighted the non-spontaneous behavior for treating dye-polluted wastewater using ZnO catalyst. Also, the results display that the dye oxidation via modified Fenton system typically proceeds at 34.53 kJ mol^{-1}. This is considered as a low energy barrier. Such result is in a agreement with the results reported by Ahmadi et al. (2016) (45.84 kJmol-1) for oxidizing Reactive Yellow 84 dye by potassium peroxydisulfate and Sun et al. (2007) (53.96 kJ mol^{-1}) for *p*-nitroaniline oxidation with Fenton's reagent.

Recyclability

The superparamagnetic $Mn_{0.6}Zn_{0.4}Fe_2O_4$ catalyst stability and recyclability is considered a superior importance for its long-term applicability in the field of wastewater treatment. Heterogeneous $Mn_{0.6}Zn_{0.4}Fe_2O_4$ based catalysts are an excellent example as a long-term catalyst reusability example since they possess an excellent magnetic characteristic. Thus, their ability for separation could be easily applicable from the reaction medium after Fenton's reaction through an external magnet. After the catalyst separation, it is subjected for successive washing with distilled water then followed by oven drying (105 °C) (Tony 2021b; Tony and Lin 2020b). Then, the recovered and regenerated catalyst is used and the mechanism is repeated. The results displayed in Fig. 11 demonstrated that a well catalytic activity is achieved during the range of experimental study till the eighth cycle of catalyst reuse, which confirms the high stability of the synthesized

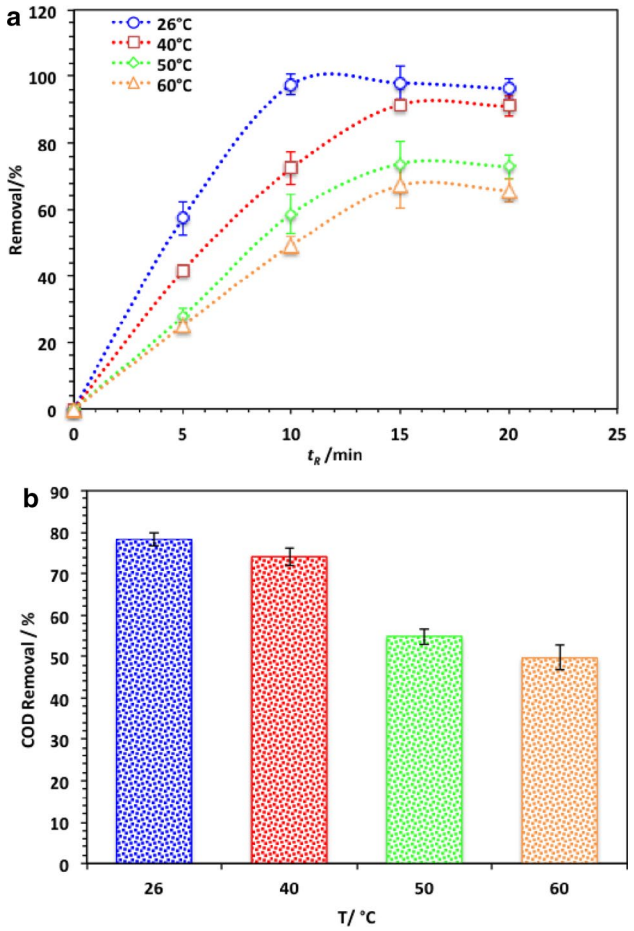

Fig. 9 Effect of temperature on Synozol Blue removal (**a**) Colour removal; (**b**) COD removal

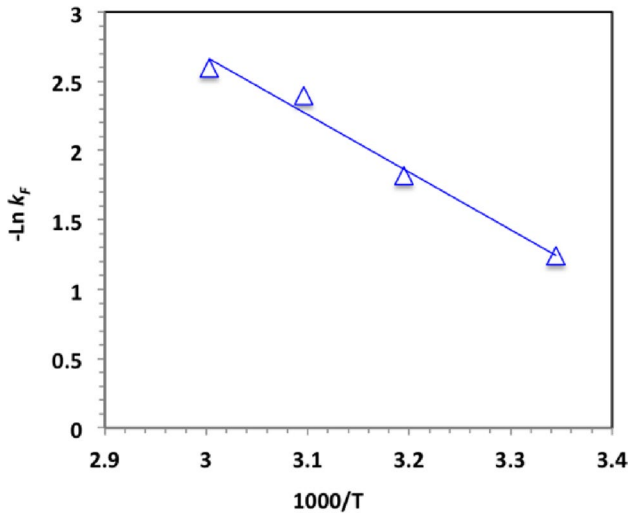

Fig. 10 Plot of ln k_F versus 1000/T for the Synozol Blue oxidation reaction (solid lines represent least-squares fitting)

Table 6 Thermodynamics parameters of Synozol Blue dye oxidation via $Mn_{0.6}Zn_{0.4}Fe_2O_4/H_2O_2/UV$

Thermodynamics Parameters	T/°C			
	26 °C	40 °C	50 °C	60 °C
Ea/kJmol^{-1}	34.54			
ΔG^o/kJmol^{-1}	76.31	81.51	85.75	89.05
ΔH^o/kJmol^{-1}	32.05	31.94	31.86	31.77
ΔS^o/Jmol^{-1}	− 148.02	− 158.38	− 166.87	− 171.99

$Mn_{0.6}Zn_{0.4}Fe_2O_4$ photocatalyst. Thus, the study verified their promising sustainability for the use in treating industrial wastewater effluents. The typical oxidation percentage of the Synozol Blue dye via superparamagnetic $Mn_{0.6}Zn_{0.4}Fe_2O_4$ based Fenton system for 8 successive cycles are presented in Fig. 11. It is worth to mention that due to the superparamagnetic catalyst features', releasing the metal ions in the aqueous solution is difficult to occur which confirms the catalyst sustainability.

Conclusion

The current study attempted to explore the applicability of Fenton process using the superparamagnetic $Mn_{0.6}Zn_{0.4}Fe_2O_4$ nanopowder for oxidizing textile dying wastewater containing Synozol Blue dye. The experimental results of the study revealed that Fenton process by magnetic catalyst could be an appropriate treatment alternative for Synozol Blue dye removal, providing high dye and COD removal efficiencies with minimum chemicals consumption. The colour and COD oxidation as target efficiencies were found to be a function of the initial pH, H_2O_2 and catalyst doses. Response surface methodology (RSM) based on central composite design (CCD) has been successfully employed for process optimization and the optimum operating values were 39 and 404 mg L^{-1} of $Mn_{0.6}Zn_{0.4}Fe_2O_4$ and H_2O_2, respectively, at 15 min of reaction at acidic pH conditions. The pseudo-first-order kinetic model is accepted to be well fitted with the experimental data. Overall, the results obtained for Synozol Blue dye removal using the $Mn_{0.6}Zn_{0.4}Fe_2O_4$ based Fenton reaction verify the significant role of the recyclable magnetic nanoparticles in oxidizing dye molecules from aqueous effluents. Such experimental data, derived from the synesthetic textile dying wastewater, add to a knowledge base for treating real textile wastewater matrix treatment applications.

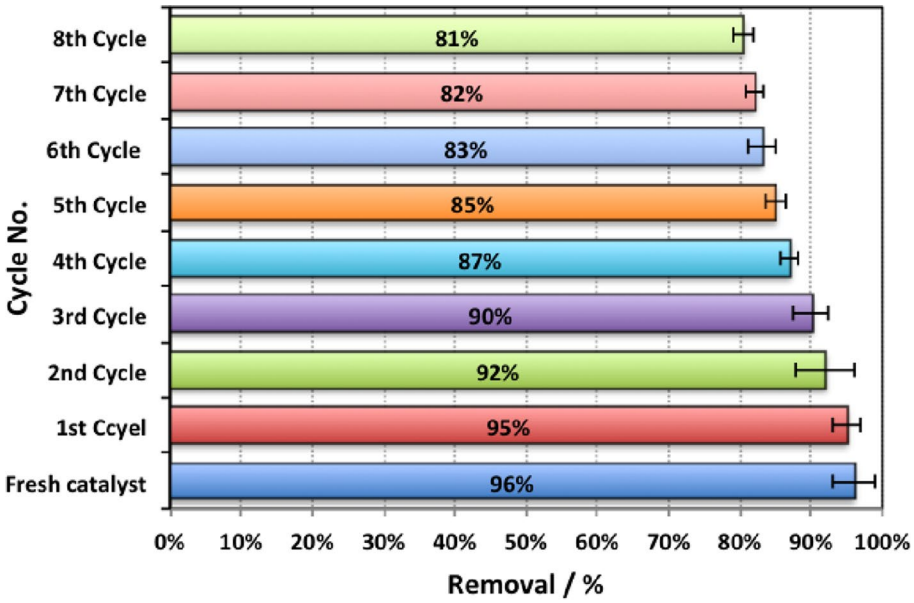

Fig. 11 Reusability of $Mn_{0.6}Zn_{0.4}Fe_2O_4$ for successive cycles use under similar conditions

Funding The author(s) received no specific funding for this work.

Availability of data and material All data generated or analysed during this study are included in this published article.

Declarations

Conflict of interest The authors confirm that there is no conflict of interest to declare.

Consent for publication The authors confirm the consent for publication.

Human and animal rights This article does not contain any studies with human or animal subjects.

References

Abdel Maksoud M, El-Sayyad G, Abokhadra A, Soliman L, El-Bahnasawy H, Ashour A (2020) Influence of Mg2+ substitution on structural, optical, magnetic, and antimicrobial properties of Mn–Zn ferrite nanoparticles. J Mater Sci Mater Electron 31:2598–2616

Abdollahzadeh H, Fazlzadeh M, Afshin S, Arfaeinia S, Feizizadeh A, Poureshgh Y, Rashtbari Y (2020) Efficiency of activated carbon prepared from scrap tires magnetized by Fe3O4 nanoparticles: characterisation and its application for removal of reactive blue19 from aquatic solutions. Int J Environ Anal Chem. https://doi.org/10.1080/03067319.2020.1745199

Ahmadi M, Behin J, Mahnam AR (2016) Kinetics and thermodynamics of peroxydisulfate oxidation of Reactive Yellow 84. J Saudi Chem Soc 20:644–650

Al Momani F, Shawaqfah M, Shawaqfeh A, Al-Shannag M (2008) Impact of Fenton and ozone on oxidation of wastewater containing nitroaromatic compounds. J Environ Sci 20:675

Argun ME, Karatas M (2011) Application of Fenton process for decolorization of reactive black 5 from synthetic wastewater: kinetics and thermodynamics. Prog Sust Energy 30:540

Ashour E, Tony MA (2020) Eco-friendly removal of hexavalent chromium from aqueous solution using natural clay mineral: activation and modification effects. SN Appl Sci 2:2042. https://doi.org/10.1007/s42452-020-03873-x

Ashour E, Tony MA (2017) Equilibrium and kinetic studies on biosorption of iron(II) and iron(III) ions onto eggshell powder from aqueous solution. Appl Eng 1(3):65–73

Ashour EA, Tony MA, Purcell PJ (2014) Use of agriculture-based waste for basic dye sorption from aqueous solution: kinetics and isotherm studies. Am J Chem Eng 2:92–98. https://doi.org/10.11648/j.ajche.20140206.14

Bayantong ARB, Shih Y, Ong DC, Abarca RM, Dong C, de Luna M (2021) Adsorptive removal of dye in wastewater by metal ferrite-enabled graphene oxide nanocomposites. Chemosphere 274:129518. https://doi.org/10.1016/j.chemosphere.2020.129518

Bia X, Wanga P, Jiao C, Cao H (2009) Degradation of remazol golden yellow dye wastewater in microwave enhanced ClO2 catalytic oxidation process. J Hazard Mater 168:895–900

Boretti A, Rosa L (2019) Reassessing the projections of the World Water Development Report. Npj Clean Water 2:15. https://doi.org/10.1038/s41545-019-0039-9

Chen R, Pignatello JJ (1997) Role of quinone intermediates as electron-shuttles in Fenton and photoassisted Fenton oxidations of aromatic compounds. Environ Sci Technol 31:2399–2406

Eltabey MM, Massoud AM, Radu C (2017) Amendment of saturation magnetization, blocking temperature and particle size

homogeneity in Mn-ferrite nanoparticles using Co-Zn substitution. Mater Chem Phys 186:505–512
Ercin AE, Hoekstra AY (2014) Water footprint scenarios for 2050: A global analysis. Environ Int 64:71–82
Fang M, Tan X, Liu Z, Hu B, Wang X (2021) Recent progress on metal-enhanced photocatalysis: a review on the mechanism, AAAS Research, 2021: Article ID 9794329, 16 pages, https://doi.org/10.34133/2021/9794329
Garcia-Muñoz P, Fresno F, O'shea V, Keller N (2020) Ferrite materials for photoassisted environmental and solar fuels applications. Topic Curr Chem. https://doi.org/10.1007/s41061-019-0270-3.hal-02413062
Ghaneian A, Khavanin A, Hashemian SJ, Moussavi G, Ghanizadeh G, Hajizadeh E (2008) Photochemical oxidation of reactive blue 19 dye (RB19) in textile wastewater by UV/K2S2O8 process. Iran J Environ Health Sci Eng 5(2):95–100
Guede A, Madeira AM, Boaventura LM, Costa CA (2003) Fenton oxidation of cork cooking wastewater–overall kinetic analysis. Water Res 37:3061. https://doi.org/10.1016/S0043-1354(03)00178-7
He F, Lei L (2004) Degradation kinetics and mechanisms of phenol in photo-Fenton process. J Zhejiang Univ Sci 5(2):198–205. https://doi.org/10.1631/jzus.2004.0198
Ilyas S, Abdul Rehman A (2013) Decolorization and detoxification of Synozol red HF-6BN azo dye, byAspergillus niger and Nigrospora sp. Iranian J Environ Health Sci Eng 10(1):12. https://doi.org/10.1186/1735-2746-10-12
Ilyas S, Bukhari DA, Rehman A (2015) Decolorization of synozol red 6HBN by yeast, candida tropicalis 4S, isolated from industrial wastewater. Pak J Zool 47(4):1181–1185
Ioannou LA, Fatta-Kassinos D (2013) Solar photo-Fenton oxidation against the bioresistant fractions of winery wastewater. J Environ Chem Eng 1:703–712. https://doi.org/10.1016/j.jece.2013.07.008
Khan M, Siddique M, Wahid F, Khan R (2015) Removal of reactive blue 19 dye by sono, photo and sonophotocatalytic oxidation using visible light. Ultras Sonochem 26:370–377
Khedher M, Mossad M, El-Etriby H (2017) Treatment of colored wastewater from textile industry using electrocoagulation process. Mansoura Eng J 42(1110):0141
Li K, Peng C, Jiang K (2011) The recycling of Mn–Zn ferrite wastes through a hydrometallurgical route. J Hazard Mater 194:79–84
Li Q, Chen Z, Wang H, Yang H, Wen T, Wang S, Hu B, Wang X (2021a) Removal of organic compounds by nanoscale zero-valent iron and its composites. Sci Total Environ 792:148546
Li B, Hu Y, Shen Z, Ji Z, Yao L, Zhang S, Zou Y, Tang D, Qing Y, Wang S, Zhao G, Wang X (2021b) Photocatalysis driven by near-infrared light: materials design and engineering for environmentally friendly photoreactions. ACS EST Engg 1(6):947–964. https://doi.org/10.1021/acsestengg.1c00103
Liu X, Pang H, Liu H, Li Q, Zhang N, Mao L, Qiu M, Hu B, Yang H, Wang X (2021) Orderly porous covalent organic frameworks-based materials: superior adsorbents for pollutants removal from aqueous solutions. Innov 2(1):100076
Maroudas A, Pandis PK, Chatzopoulou A, Davellas LR, Sourkouni G, Argirusis C (2021) Synergetic decolorization of azo dyes using ultrasounds, photocatalysis and photo-fenton reaction. Ultrason Sonochem 71:105367. https://doi.org/10.1016/j.ultsonch.2020.105367
Muda K, Aris A, Salim MR, Ibrahim Z, Yahya A, van Loosdrecht MC, Ahmad A, Nawahwi MZ (2010) Development of granular sludge for textile wastewater treatment. Water Res 44(15):4341–4350
Najjar W, Chirchi L, Santos E, Ghorhel A (2001) Kinetic study of 2-nitrophenol photodegradation on Al-pillared montmorillonite doped with copper. J Environ Monitor 3(6):697–701
Neamtu M, Siminiceanu I, Yediler A, Kettrup A (2002) Kinetics of decolorization and mineralization of reaction azo dyes in aqueous solution by the UV/H2O2 oxidation. Dyes Pig 53:93–99
Pintor AM, Vilar VJ, Boaventura RA (2011) Decontamination of cork wastewaters by solar-photo-fenton process using cork bleaching wastewater as H_2O_2 source. Sol Energy 85:579–587. https://doi.org/10.1016/j.solener.2011.01.003
Pourali P, Behzad M, Arfaeinia H, Ahmadfazeli A, Afshin S, Poureshgh Y, Rashtbari Y (2020) Removal of acid blue 113 from aqueous solutions using low-cost adsorbent: adsorption isotherms, thermodynamics, kinetics and regeneration studies. Sep Sci Technol 56(18):3079–3091. https://doi.org/10.1080/01496395.2020.1867583
Ramirez J, Maldonado-Hódar F, Pérez-Cadenas A, Moreno-Castilla C, Costa C (2007) Madeira L (2007) azo-dye orange II degradation by heterogeneous Fenton-like reaction using carbon-Fe catalysts. Appl Catal B 75:312–323
Rath C, Sahu KK, Anand S, Date SK, Mishra NC, Das RP (1999) Preparation and characterization of nanosize Mn–Zn ferrite. J Mag Mag Mater 202(1):77–84
Rezaee A, Ghaneian MT, Khavanin A, Hashemian SJ, Moussavi GH (2008) Photochemical oxidationof reactive blue 19 dye (RB19) in textile wastewater by UV/K2S2O8 process. J Environ Heal Sci Eng 5(2):95-100
Rezgui S, Díez A, Monser L, Adhoum N, Pazos M (2021) Angeles Sanromán, ZnFe2O4-chitosan magnetic beads for the removal of chlordimeform by photo-Fenton process under UVC irradiation. J Environ Manag 283:111987
SAS/STAT, User's Guide (SAS Institute, Inc., Cary, NC, 1990)
Shanmugam BK, Easwaran SN, Mohanakrishnan AS, Kalyanaraman C, Mahadevan S (2019) Biodegradation of tannery dye effluent using Fenton's reagent and bacterial consortium: a biocalorimetric investigation. J Environ Manage 15(242):106–113. https://doi.org/10.1016/j.jenvman.2019.04.075 (**Epub 2019 Apr 24 PMID: 31028950**)
Sharma R, Bansalb S, Sonal Singh S (2015) Tailoring the photo-Fenton activity of spinel ferrites (MFe_2O_4) by incorporating different cations (M ¼ Cu, Zn, Ni and Co) in the structur. RSC Adv 5:6006
Sun J-H, Sun S-P, Fan M-H, Guo H-Q, Qiao L-P, Sun R-X (2007) A kinetic study on the degradation of p-nitroaniline by Fenton oxidation process. J Hazard Mater 148(1–2):172–177. https://doi.org/10.1016/j.jhazmat.2007.02.022
Tamimi M, Qourzal S, Barka N, Assabbane A, Ait-Ichou A (2008) Methomyl degradation in aqueous solutions by fenton's reagent and the photo-fenton system. Sep Purif Technol 61(1):103–108
Tayeb AM, Tony MA, Ismaeel EK (2019) Engineered nanostructured ZnO for water remediation: operational parameters effect, Box-Behnken design optimization and kinetic determinations. Appl Water Sci 9:43. https://doi.org/10.1007/s13201-019-0921-0
Thabet RH, Tony MA, El Sherbiny SA, Ali IA, Fouad MK (2020) Catalytic oxidation over nanostructured heterogeneous process as an effective tool for environmental remediation. IOP Conf Ser Mater Sci Eng 975:012004
Thabet RH, Fouad MK, Ali IA, El Sherbiny SA, Tony MA (2021a) Magnetite- based nanoparticles as an efficient hybrid heterogeneous adsorption/oxidation process for reactive textile dye removal from wastewater matrix. Int J Environ Anal Chem. https://doi.org/10.1080/03067319.2021.189671
Thabet RH, Fouad MK, Ali IA, El Sherbiny SA, Tony MA (2021b) Synthesis, characterization and potential application of magnetized nanoparticles for photocatalysis of levafix CA Reactive Azo-Dye in aqueous effluent. Water Environ J. https://doi.org/10.1111/wej.12756
Thakur P, Chahar D, Taneja S, Bhalla N, Thakur A (2020) A review on MnZn ferrites: synthesis, characterization and applications. Ceram Int 46:15740–15763
Tian T, Yu H (2020) Iron-assisted biological wastewater treatment: synergistic effect between iron and microbes. Biotechnol Adv.

https://doi.org/10.1016/j.biotechadv.2020.107610 (**Epub 2020 Aug 16**)

Tony MA (2020a) Central composite design optimization of Bismarck Dye oxidation from textile effluent with Fenton's reagent. Appl Water Sci 10(5):108

Tony MA (2020b) Zeolite-based adsorbent from alum sludge residue for textile wastewater treatment. Int J Environ Sci Technol 17:2485–2498. https://doi.org/10.1007/s13762-020-02646-8

Tony MA (2021a) Low-cost adsorbents for environmental pollution control: a concise systematic review from the prospective of principles, mechanism and their applications. J Disp Sci Technol. https://doi.org/10.1080/01932691.2021.1878037

Tony MA (2021b) An industrial ecology approach: green cellulose based bio-adsorbent from sugar industry residue for treating textile industry wastewater effluent. Int J Environ Anal Chem 101(2):167–183

Tony MA (2021c) Solar concentration for green environmental remediation opportunity— International review: advances, constraints and their practice in wastewater treatment. Inter J Environ Anal Chem. https://doi.org/10.1080/03067319.2021.1895138

Tony MA (2021d) Paradigms of homo/heterogonous Fenton systems for "emerging pollutants" removal—limitations and advancements. Int J Environ Anal Chem. https://doi.org/10.1080/03067319.2021.1977287

Tony MA, Lin LS (2020a) Performance of acid mine drainage sludge as an innovative catalytic oxidation source for treating vehicle-washing wastewater. J Disp Sci Technol. https://doi.org/10.1080/01932691.2020.1813592

Tony MA, Lin LS (2020b) Attenuation of organics contamination in polymers processing effluent using iron-based sludge: process optimization and oxidation mechanism. Environ Technol. https://doi.org/10.1080/09593330.2020.1803417

Tony MA, Lin LS (2021) Iron coated-sand from acid mine drainage waste for being a catalytic oxidant towards municipal wastewater remediation. Int J Environ Res 15:191–201

Toosi FS, Hosseiny M, Joghataeic A, Toosi FS (2017) The Application of Sio_2Nanoparticles for Anionic Dye Removal from Aqueous Solution. Arch Hyg Sci 6(2):136–144

Torrades F, García-Montano J (2014) Using central composite experimental design to optimize the degradation of real dye wastewater by Fenton and photo-Fenton reactions. Dyes Pigments 100:184–189

Vinosha PA, Das SJ (2018) Investigation on the role of pH for the structural, optical and magnetic properties of cobalt ferrite nanoparticles and its effect on the photo-fenton activity. Mater Today Proc 5(2):8662–8671

Wang C, Sun R, Huang R, Cao Y (2021) A novel strategy for enhancing heterogeneous Fenton degradation of dye wastewater using natural pyrite: kinetics and mechanism. Chemosphere. https://doi.org/10.1016/j.chemosphere.2021.129883

Xuan Y, Li Q, Yang G (2007) Synthesis and magnetic properties of Mn–Zn ferrite nanoparticles. J Mag Mag Mater 312(2):464–469

Yang L, Zhang Y, Liu X, Jiang X, Zhang Z, Zhang T, Zhang L (2014) The investigation of synergistic and competitive interaction between dye Congo red and methyl blue on magnetic MnFe2O4. Chem Eng J 246:88–96

Zafar Z, Ali I, Park S, Kim J (2020) Effect of different iron precursors on the synthesis and photocatalytic activity of Fe–TiO2 nanotubes under visible light. Ceram Int 46:3353. https://doi.org/10.1016/j.ceramint.2019.10.045

Zhao YQ, Keogh C, Tony MA (2009) On the necessity of sludge conditioning with non-organic polymer: AOP approach. Res Sci Technol 6:151–155

Zou R, Angelidaki I, Yang X, Tang K, Andersen H, Zhang Y (2020) Degradation of pharmaceuticals from wastewater in a 20-L continuous flow bio-electro-Fenton (BEF) system. Sci Total Environ 727:138684

Zou Y, Hu Y, She Z, Yao L, Tang D, Zhang S, Wang S, Hu B, Zhao G, Wang X (2022) Application of aluminosilicate clay mineral-based composites in photocatalysis. J Environ Sci 115:190–214